SSCL-Preprint-556
February 1994
Distribution Category: 400

A. Drozhdin
N. Mokhov
B. Parker

Accidental Beam Loss in Superconducting Accelerators: Simulations, Consequences of Accidents and Protective Measures

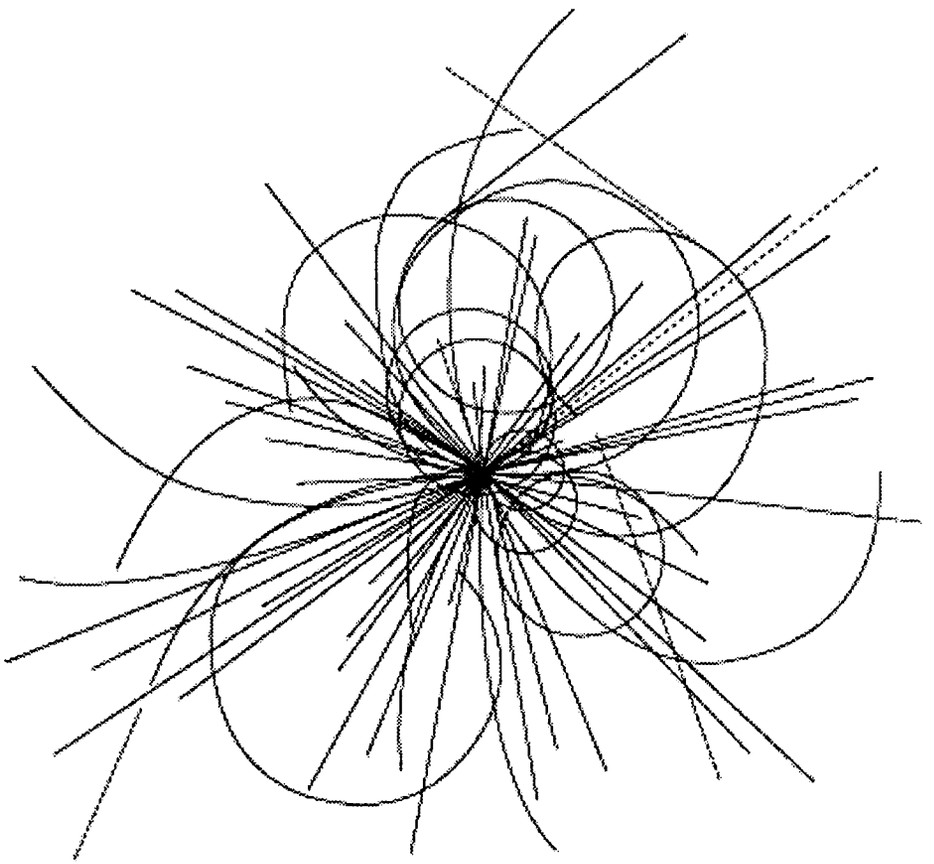

Superconducting Super Collider Laboratory

SSCL-Preprint-556

Accidental Beam Loss in Superconducting Accelerators: Simulations, Consequences of Accidents and Protective Measures*

A. Drozhdin, N. Mokhov, and B. Parker

Superconducting Super Collider Laboratory†
2550 Beckleymeade Ave.
Dallas, TX 75237, USA

February 1994

*To be submitted to the *Journal of Nuclear Instruments and Methods in Physics Research.*

†Operated by the Universities Research Association, Inc., for the U.S. Department of Energy under Contract No. DE-AC35-89ER40486.

Accidental Beam Loss in Superconducting Accelerators: Simulations, Consequences of Accidents and Protective Measures

A. Drozhdin, N. Mokhov, and B. Parker

Abstract

The consequences of an accidental beam loss in superconducting accelerators and colliders of the next generation range from the mundane to rather dramatic, *i. e.*, from superconducting magnet quench, to overheating of critical components, to a total destruction of some units via explosion. Specific measures are required to minimize and eliminate such events as much as practical. In this paper we study such accidents taking the Superconducting Supercollider complex as an example. Particle tracking, beam loss and energy deposition calculations were done using the realistic machine simulation with the Monte-Carlo codes MARS12 and STRUCT. Protective measures for minimizing the damaging effects of prefire and misfire of injection and extraction kicker magnets are proposed here.

1. Introduction

The circulating beam energy at future high intensity accelerators is high enough to cause severe damage to the equipment. The Superconducting Super Collider (SSC) beam would have contained approximately 420 MJ of circulating beam energy per ring at the operating design point of 20 TeV/c and 70 mA [1]. This energy is equivalent to that stored in about 100 kg of high explosives. The Collider abort system uses fast extraction to divert the beam to a massive graphite absorber for normal termination of the operating cycle or in any of a number of predefined fault modes. The abort kicker magnet system consists of 24 pulsed magnets having a rise time of about 3 μs. Normally this system is triggered during the 4 μs "abort gap" in the circulating beam. If any kicker prefires or misfires, some fraction of the beam may not reach the absorber. Accidental beam loss consequences in the Collider range from superconducting magnet quenches, to overheating of some components, to total destruction of some units through their explosion [2, 3]. The situation is similar in the High Energy Booster (HEB), the 2 TeV superconducting injector to the Collider, and for other machines under design (LHC, TESLA *etc.*). Specific measures are required to mitigate and possibly to eliminate such events [4, 5]. In this paper we further study such accidents. Material heating and radiation generation are studied using full scale machine simulations with STRUCT code [6] and Monte-Carlo energy deposition calculations with MARS12 [7]. Protective measures for minimizing the damaging effects of prefires and misfires are then proposed. These Supercollider and HEB results are applicable to other accelerators of such scale.

2. Beam collimation system and shadow protectors

To provide reliable operation of a superconducting accelerator and collider experiments a multi-component beam collimation system must be incorporated in the machine [8-10]. For the Collider, collimator locations in the West Utility and Interaction Regions (IRs) are presented in figs. 1 and 2 and table 1 [9]. These collimators are positioned at 20σ with

respect to the Collider closed orbit. The admittance of the machine is 729 mm.mrad or 27σ of the circulating beam at the top energy, *i.e.*, collimators are placed only 7σ inside the physical aperture of the Collider. During a beam misbehavior, even a small portion of the beam is enough to destroy any small aperture component. These are, first of all, septa of the Lambertson magnets, scrapers and collimators. The longitudinal distribution of peak temperature in a septum is shown in fig. 3 for an unsynchronized abort of a 20-TeV beam. One sees that the first meter of the steel septum would be instantaneously melted.

To protect components, one can utilize a specific feature of beam-induced shower development in the TeV region, *i.e.*, that the energy deposition density at cascade maximum is determined by electromagnetic showers, induced by π^0-decays [11]. Consequently, the peak energy deposition in light materials is lower than in heavy ones proportionally to a power of the Z-ratio. We find that the best solution is to put a graphite shadow right in front of a critical component. The shadow piece is an inert device with an aperture the same as that of the adjacent component which it is protecting. In fig. 3 we show that the expected temperature profile in graphite is quite different from that found in steel, with a peak temperature of about 800 °C. The length of a shadow shield is chosen to contain most of a cascade that is 5 meters at 20 TeV. Another criterion to the shadow length is that an instantaneous peak temperature in the downstream component must be below some limit, which we take to be 500 °C for steel. The longitudinal distribution of temperature in the CGWUT2 shadow/collimator pair immediately after an unsynchronized beam abort is shown in fig. 4. Peak temperature in the steel section is reduced to 380 °C, whereas it is almost 900 °C in the 4-m long graphite shadow.

At lower energies, the situation becomes much more favorable; a 2 TeV unsynchronized abort in the Collider results in a maximum temperature rise in the steel septum of 450 °C "only." In the HEB it is 550 °C in the collider mode, but is still well

above a steel melting point for the test beam intensity 10^{14} ppp, so again a graphite shadow of about 3-m length is required.

3. Abort kicker prefire and unsynchronized abort

The abort kicker prefire results in high amplitude coherent betatron oscillations of the beam. The disturbed beam can then induce collimator jaws overheating up to hundreds of degrees centigrade. Again the worst situation in the Collider takes place at 20 TeV. Simulation of this process has been done with the following assumptions: circulating beam has been cleaned up to the 10σ level by the scraper, 99% of the circulating beam is inside the 4σ region, and 1% of the beam is between 4 and 10σ. In the worst case, when prefire of an abort kicker takes place just after the longitudinal abort gap, one needs to wait one turn to abort the beam. The overheating of the IR collimator CLESIRT exceeds considerably the steel melting point. To avoid overheating of this collimator one should decrease the interval of time between a prefire and the start of the next 23 kickers to less than 5 μs. Unfortunately, the kicker pulse rise time is unlikely to be contained within the gap in the longitudinal distribution of the circulating beam (unsynchronized abort). Results of a simulation of beam loss during the 3 μs kicker rise time are presented in fig. 5. At kicker low field level, halo particles are intercepted by the collimator CLESIRT in the IR. The calculated temperature profile is shown in fig. 6 for the innermost collimator surface and 1.5 mm deep in the collimator body. The maximum temperature rise in this collimator is 400 °C. At a level of about 10% of kicker strength the deflected beam is intercepted by a graphite shadow in front of the second collimator in the West Utility (see figs. 1 and 4). At about 40% level of kicker strength, the beam is intercepted by the graphite shadow of the Lambertson magnet (fig. 3).

There are two ways proposed to decrease the overheating of collimators and shadows:

• Decrease the abort kicker rise time from 3 μs to 1 μs yielding a 3-fold decrease in heating;

• Compensate a prefired kicker via a module with the opposite magnetic field (antikicker). In this case the beam abort can be safely delayed until the abort gap, thus eliminating beam loss during the kicker rise time.

Recent simulations performed at SSCL suggest that the dynamic aperture of the Collider at the top energy is equal to about 12σ and the lifetime of the particles with large betatron amplitudes, from 12 to 20σ, varies from 50 to 2 turns, respectively [12]. The lifetime is lower than one turn at amplitudes greater than 20σ. For this case, collimator jaws should be installed between 16–20σ from the circulating beam axis to protect superconducting magnets against irradiation. Such a collimator would intercept a denser part of the circulating beam. This closer position causes a 10-fold increase in overheating as compared to the 20σ position and the overheating of the collimator CLESIRT jaw during an unsynchronized abort is thus increased to an inadmissible temperature of 900 °C. The kicker risetime reduction method, outlined above, is ineffective in this case, and only an antikicker method is viable. For the second method, the collimator jaw overheating is strongly dependent upon the delay between prefire and start of the antikicker. The resulting kick and beam loss as a function of time for different delays (1.2 μs and 1.65 μs) are presented in figs. 7 and 8. With a 1.8 μs delay, the resulting kick exceeds 75% of that for a single kicker and the collimator CLESIRT overheating exceeds the steel melting point. Collimator jaws overheating as a function of antikicker delay is shown in fig. 9. An acceptable temperature rise of about 300 °C is exceeded for a 1.5 μs delay between a prefire of the abort kicker and a start of the antikicker. We therefore conclude that ensuring a short (<1.5 μs) delay is an important antikicker design requirement. Our simulations show that for large (>20σ) collimator settings, an unsynchronized abort is allowable if graphite shadows are used upstream of the abort Lambertson magnet and second collimator in the West Utility. For smaller collimator settings (between 16 and 20σ) an antikicker with less than 1.5 μs delay is needed to reduce Collider equipment overheating to tolerable levels.

4. HEB extraction kicker misfire

The smallest apertures in the HEB-Collider transfer lines are situated at the upstream end of the first HEB Lambertson magnet and at the downstream end of the Collider injection Lambertson magnet (figs. 10, and 11). Extracted beam axis comes to within 5 mm of the HEB and Collider Lambertson magnet aperture limits, and 3.7 mm from the superconducting quadrupoles Q1 and QU3B apertures. The circulating beam passes through the "field free" hole of the Lambertson magnets 6 mm from the aperture edge. Note that the horizontal beam size, at 3σ level, is equal to 1.5 mm and 1.7 mm in these magnets.

Misfire of a HEB extraction kicker sends in the extracted beam displacement closer to the septum of both the HEB and Collider Lambertson magnets. Results from our numerical simulations of the HEB kicker misfire are shown in figs. 12 and 13 for two extracted beam positions at the HEB and Collider level. The beam axis is 5 mm away from the Lambertson magnet aperture and 3 mm from the superconducting quadrupoles Q1 and QU3B apertures as shown in fig. 12. The beam is moved 0.7 mm closer to the Collider Lambertson magnet aperture in fig. 13. Beam loss is shown as a function of the beam+halo dimension. The extracted beam consists of 4σ beam core and halo with 1% of the beam intensity outside the 4σ size. Beam loss in QU3B and Q1 quadrupoles is shown in the same pictures during normal operation without any kicker misfire.

Displacement of the beam closer to the septum leaves the beam loss in the Lambertson magnets and collimator CLENIRT essentially unchanged, but eliminates particle loss in the superconducting quadrupoles Q1 and QU3B. The collimator CLENIRT and the HEB Lambertson magnet overheating remains below 100 °C with the HEB scraper positioned at $d = 14\sigma$ distance from the beam axis. Beam loss during normal operation, as shown in fig. 12, exceeds the fast quench level (3×10^7 protons per meter for the HEB and 3×10^6 protons/m for the Collider quadrupoles) at $d = 12\sigma$. Therefore, one needs to ensure that the

injected beam does not pass closer than 3.7 mm to the QU3B and Q1 apertures during injection.

5. Collider injection kicker misfire and prefire

A prefire of any one of the five injection kickers results in a coherent betatron oscillation of 1/8 of a full Collider fill with a circulating beam amplitude of about 5 mm with respect to the closed orbit. Beam halo particles intercepted by the Collider elements induce overheating of superconducting magnets. Misfire of the injection kicker causes the same problem with the injected beam from the transfer line.

The rms closed orbit distortion at injection is equal to 1 mm in the Collider arc sections. Maximum β-function at injection is as high as 650 m in QL2A, QL2B, QL3A, QL3B of IRs and diameter of aperture is equal to 42 mm. Displacement of the beam here, because of a beam separation, is equal to about 5 mm. The beam pipe is as close as 16 mm to the circulating beam axis. There are eight such locations spread through the Collider lattice, so, it is difficult to keep the closed orbit of the beam within limit at every location. The Collider admittance determined following this consideration is equal to 290 mm.mrad or 17σ of circulating beam. Collimator jaws should be positioned at $16–17\sigma$ from the beam axis to protect superconducting magnets against irradiation. Having collimators moved closer to the beam will increase the danger of collimator jaws overheating at abort and injection prefire or misfire.

In the case of an injection kicker misfire or prefire, the circulating beam must be aborted out of the Collider during the next few turns, because the transverse damping system cannot damp such a large injection beam displacement to an acceptable level. The following injection error scenario has been investigated. The HEB extracted beam passes through the beam transfer line to the Collider, where it remains six turns before being aborted through

the beam abort line to the backstop. Collimator jaws are positioned at 16σ with respect to the beam axis. Some additional assumptions are:

• 1% of the circulating beam is inside the region of 4 to 10σ of the beam (halo definition);

• $\Delta B/B$ of the abort kicker is equal to +12.5% (due to abort design for vertical painting);

• A full 1/8 of the circulating beam protons are effected by the injection kicker.

Four cases of an injection kicker scheme with the above assumptions have been investigated: the kicker system segmented into 5, 6, 7 or 8 modules. Total strength of the whole kicker system is kept fixed for all four cases. For the baseline 5 kicker scenario, beam loss in the first superconducting dogleg magnet in the West Utility results in a quench of that magnet with a peak instantaneous temperature rise of about 60 °C in case of ID = 32.7 mm diameter of its beam pipe aperture. With ID = 42 mm, calculated beam loss is below the fast quench limit.

The positions of the circulating and the aborted beam upstream of the Lambertson shadow are shown in fig. 14. A portion of the aborted beam is intercepted by the shadow, but the graphite shadow overheating remains below 3 °C. The collimator overheating for prefire and misfire of the injection kicker versus jaw position is presented in fig. 15 for the 5 module case. The strong dependence of the maximum instantaneous temperature rise on the collimator jaw position suggests caution in the choice of the number of injection kicker modules. The collimator overheating for 6 modules versus jaw position is shown at fig. 16. The dependence on the kicker module number is presented in fig. 17. One concludes that in order to eliminate Collider equipment overheating at injection one needs to increase the number of injection kicker modules from the baseline 5 to at least 6 modules.

6. Injection kicker timing error

Large injection kicker timing errors will result in serious problems for the unprotected superconducting equipment. For this reason, a few collimators in the HEB and Collider collimation systems are dedicated to such events [9, 10]. But even at the lowest energy considered—200 GeV beam injected to the HEB—the overheating of some steel collimators can be unacceptably high (>1000 °C). So, a 1.5-m long graphite shadow followed by 0.5-m steel collimator should be incorporated into the HEB system instead of a purely metal unit.

Let's assume that the time mismatch of the kicker magnetic field pulse takes place during the commissioning period when unsynchronized injection is to be expected. Then in the Collider, the number of 2 TeV protons in the injected beam is 1.6×10^{13}. For lower intensity during actual commissioning, one can simply rescale the results of the simulation accordingly. The HEB extraction kicker rise time duration is equal to 1.5 μs (fig. 18). The HEB abort gap is only 0.2 μs longer. Kicker pulse time error causes loss of the beam both in the HEB Lambertson magnet septa and in the transfer line collimator.

At 33% of the full kicker strength the beam passes close to the septum inside the field free region of the Lambertson magnet, leading to the first peak in a beam loss distribution shown in fig. 19. The beam loss reaches the maximum at 42% of the kicker strength, at which point the whole beam is intercepted by the Lambertson's septa. Beyond 54% of the kick the beam loss goes down, but beam loss in the transfer line collimator appears and goes up. The function of this collimator is to protect the Collider at two kicker modules misfire [5]. Beam loss reaches the maximum at 62% of kick and goes down to zero at 80% of the kicker strength. Beam loss in the Lambertson magnet is 1.4×10^{11} protons and in the collimator 9×10^{10} protons. This results in an instantaneous temperature rise the Lambertson magnet coils of 700 °C at peak. For HEB extraction kicker timing errors, beam

loss in the Collider Lambertson magnet is three orders of magnitude lower and there is no meaningful loss in the downstream magnets.

Collider injection kicker timing errors cause the loss of circulating and injected beam particles (fig. 20). Circulating beam, deflected by the mismatched kicker, hits the inward side of the beam pipe. If the kicker is off, the newly injected beam heats the outward side of the beam pipe. At 25% of the kicker strength, beam loss arises in the IR collimators. These collimators are assumed placed at 16σ position from the circulating beam axis at injection. A beam loss location depends on the kicker strength (fig. 21). At 55% of the kick the beam loss location is moved closer to the kicker position. A few superconducting magnets are heated by the beam during the remaining rise up to 100%; however, only a few magnets are heated simultaneously. At 100% of the kick the whole beam hits the second and third superconducting dipoles downstream QSD1 (fig. 22). These dipoles will be immediately melted. The overheating of the IR superconducting magnets and collimators during kicker rise time is about 300 °C.

The injected beam, deflected by 100% of kick, is placed on the Collider closed orbit without any loss. Beam loss in the IR collimators will start at kicker fall to 75% of the kicker strength. With a kick less than 45%, the beam loss location is moved closer to the kicker position. If the kicker is off, the injected beam heats the same two superconducting magnets, but on the opposite side of the beam pipe. These magnets are melted again. Overheating of the collimator CLENIRT is equal to 800 °C. To protect the above first two superconducting magnets against destruction at the catastrophic kicker time errors, we propose to put a two-jaw graphite collimator just upstream the quadrupole QSD1. This collimator consists of 2.8-m long graphite jaws followed by 1-m long steel jaws.

Two important conclusions are:

1. The beam loss due to kicker timing errors causes Collider equipment melting at the HEB intensity of 1.6×10^{13} protons/cycle. About 80% of the beam can hit just one superconducting magnet; therefore during commissioning, the maximum tolerable intensity is 8×10^{10} protons per beam.

2. At the full HEB intensity of 1.6×10^{13} protons/cycle, and with a kicker error less than 0.7 μs, the perturbed beam is intercepted by the collimators CLENIRT, CVENIRT, CHTIT, CLESIRT and CVESIRT in IR. The peak temperature rise in these collimators ranges from 300 to 800 °C. With a time mismatch of more than 0.7 μs, a few superconducting magnets can be overheated to these same temperatures with dramatic consequences for the cryogenic system. Errors of less than 10% of the kicker strength (or 0.15 μs time error) do not effect significantly the beam loss in the Collider. Therefore, timing errors at the normal operating mode should be much less than 0.15 μs. This requirement only takes into account the radiation problem at injection, independently from any emittance growth considerations.

The beam loss in the Collider collimators and superconducting magnets at normal operation and unpredictable accidents, calculated in this work and in paper [9], are summarized in table 2. A pedestal of 3×10^3 protons-per-meter-per-second due to beam-gas interactions [9, 13] should be added to these values.

7. Conclusions

We have investigated the consequences of accidental beam loss in superconducting accelerators. Our Monte Carlo simulations of the SSC and HEB machine lattices, made with the MARS12 and STRUCT codes, verify that the consequences of accidental beam loss are indeed rather dramatic for unprotected machines. We found simple protective measures to mitigate such events. These measures typically include the introduction of

shadow collimator/masking placed directly in front of critical components. For the injection kicker system we find it adequate to increase its degree segmentation from 5 to 6 independent modules. Finally, for the special case of prefire of an abort kicker module, an additional measure, the introduction of an antikicker module, is suggested. The results of this paper should be applicable to the future accelerators, *e.g.*, the LHC and TESLA machines.

8. Acknowledgements

We wish to thank R. Meinke, R. Richardson, R. Schailey, R. Soundranayagam, and F. H. Wang for many useful discussions during the course of this work.

9. References

[1] "Site-Specific Conceptual Design of the Superconducting Super Collider," SSC Lab, July 1990.

[2] I. Baishev, A. Drozhdin, and N. Mokhov, "Beam Loss and Radiation Effects in the SSC Lattice Elements," SSCL-306 (1990).

[3] D. Wilson, C. Wingate, J. Goldstein, R. Godwin, and N. Mokhov, "Hydrodynamic Calculations of 20 TeV Beam Interactions with the SSC Beam Dump," Proc. of IEEE Particle Accelerator Conference, p. 3090 (1993).

[4] A. Drozhdin, I. Baishev, N. Mokhov, B. Parker, R. Richardson, and J.Zhou, "Dealing with Abort Kicker Prefire in the Superconducting Super Collider," SSCL-329 (1993); Proc. of IEEE Particle Accelerator Conference, p. 3772 (1993).

[5] R. Soundranayagam, A. Drozhdin, N. Mokhov, B. Parker, R. Schailey, and F. Wang, "Consequences of Kicker Failure During HEB to Collider Injection and Possible Mitigation," SSCL-358 (1993); Proc. of IEEE Particle Accelerator Conference, p. 1360 (1993).

[6] I. Baishev, A. Drozhdin, and N. Mokhov, "STRUCT Code User's Reference Manual," SSCL-MAN-0034 (1994).

[7] N. Mokhov, "MARS12 Code System," Proc. SARE Workshop, Santa Fe (1993); N.Mokhov, "MARS10 Code System User's Guide," Fermilab FN-509 (1989).

[8] M. Maslov, N. Mokhov, and I. Yazynin, "The SSC Beam Scraper System," SSCL-484 (1991).

[9] A. Drozhdin, N. Mokhov, J. Tompkins, and R. Soundranayagam, "Toward Design of the Collider Beam Collimation System," SSCL-Preprint-555 (1994).

[10] A. Drozhdin, N. Mokhov, and R. Schailey, "HEB Beam Collimation System," SSCL-662 (1994).

[11] A. Kalinovsky, N. Mokhov, and Yu. Nikitin, "Passage of High Energy Particles Through Matter," AIP, N.Y. (1989).

[12] Y. Chai, Private Communication, Available at SSCL Library, April 1993.

[13] Collider Accelerator Utility Section, Element Specification (Level 3B), SSCL Document Control # E10-000073, March 1993.

Table 1.
Summary of types and numbers of scrapers and collimators.

Name	Description	Jaw Length (m)	Shielding
SCRHWUT	Horizontal Scraper - Top Ring	1.2	0.65×4.5m
SCRVWUT	Vertical Scraper - Top Ring	1.2	
SCRHWUB	Horizontal Scraper - Bottom Ring	1.2	0.65×4.5m
SCRVWUB	Vertical Scraper - Top Ring	1.2	
CHWUT1	Horizontal - Top Ring, Warm Abort Dipole	2.8	0.35×4.5m
CHWUT2	Horizontal - Top Lambertson Magnet	2.8	0.35×4.5m
CHTIT	Horizontal - Top Hinge	2.8	0.35×4.5m
CHWUB1	Horizontal - Bottom Ring, Warm Abort Dipole	2.8	0.35×4.5m
CHWUB2	Horizontal - Bottom Lambertson Magnet	2.8	0.35×4.5m
CHTIB	Horizontal - Bottom Hinge	2.8	0.35×4.5m
CVENIRT	Vertical - Top Ring, E-N IR, BV1M	2.8	0.35×4.5m
CVESIRT	Vertical - Top Ring, E-S IR, BV1P	2.8	0.35×4.5m
CVESIRB	Vertical - Bottom Ring, E-S IR, BV1M	2.8	0.35×4.5m
CVENIRB	Vertical - Bottom Ring, E-N IR, BV1P	2.8	0.35×4.5m
CLWUT1	L-collimator - Top Ring, Dogleg Dipole	2.8	0.35×4.5m
CLWUB1	L-collimator - Bottom Ring, Dogleg Dipole	2.8	0.35×4.5m
CLENIRT	L-collimator - Top Ring, E-N IR, BV1CM	2.8	0.35×4.5m
CLESIRT	L-collimator - Top Ring, E-S IR, BV1CP	2.8	0.35×4.5m
CLENIRB	L-collimator - Bottom Ring, E-N IR, BV1CP	2.8	0.35×4.5m
CLESIRB	L-collimator - Bottom Ring, E-S IR, BV1CM	2.8	0.35×4.5m
CGWUT1	Graphite Collimator - Top Ring, QSD1	2.8	No
CGWUT2	Graphite Collimator - Top Ring, Dogleg Dipole	5.0	0.35×5.5m
CGWUB1	Graphite Collimator - Bottom Ring, QSD1	2.8	No
CGWUB2	Graphite Collimator - Bottom Dogleg Dipole	5.0	0.35×5.5m
CFENIR1	Fixed Aperture - East North IR	3.0	0.75×4.0m
CFENIR2	Fixed Aperture - East North IR	3.0	0.75×4.0m
CFESIR1	Fixed Aperture - East South IR	3.0	0.75×4.0m
CFESIR2	Fixed Aperture - East South IR	3.0	0.75×4.0m
CFENIR1	Neutral Beam Dump - East North IR	2.0	0.65×3.0m
CFENIR2	Neutral Beam Dump - East North IR	2.0	0.65×3.0m
CFESIR1	Neutral Beam Dump - East South IR	2.0	0.65×3.0m
CFESIR2	Neutral Beam Dump - East South IR	2.0	0.65×3.0m
SSWUT	Shadow Septum - Top Ring Lambertson	5.0	0.35×5.5m
SSWUB	Shadow Septum - Bottom Ring Lambertson	5.0	0.35×5.5m

Table 2.
Beam loss in the collider collimators and magnets.
3×10^3 p/m/s should be added to the rates given below.

Component	Scraping (p/m/s)	pp-collisions (p/m/s)	Unsynchro-nized Abort (p)	Abort Prefire (p)	Injection Prefire/Misfire (p)
SSWUT	1.0×10^7		1.5×10^{11}		
LAMBERTSON	1.0×10^4				
CGWUT2	7.5×10^5		3.0×10^{11}		
CHWUT1	1.5×10^5				6.0×10^9
CLWUT1	3.0×10^6				7.0×10^9
CHWUT2	7.0×10^4	3.0×10^2			
CLENIRT	1.5×10^4	7.3×10^2			1.0×10^{10}
CVENIRT	6.0×10^2	7.0×10^5			
CHTIT	2.0×10^5	2.0×10^5			8.0×10^8
CLESIRT	4.1×10^2	7.3×10^2	1.1×10^{10}	6.0×10^9	1.0×10^9
CVESIRT	6.0×10^3	7.0×10^5			
QL3A, B	8.0×10^3	3.0×10^2			
QL2A, B	2.0×10^2	2.0×10^2			
B, BS	2.0×10^2	9.0×10^3			

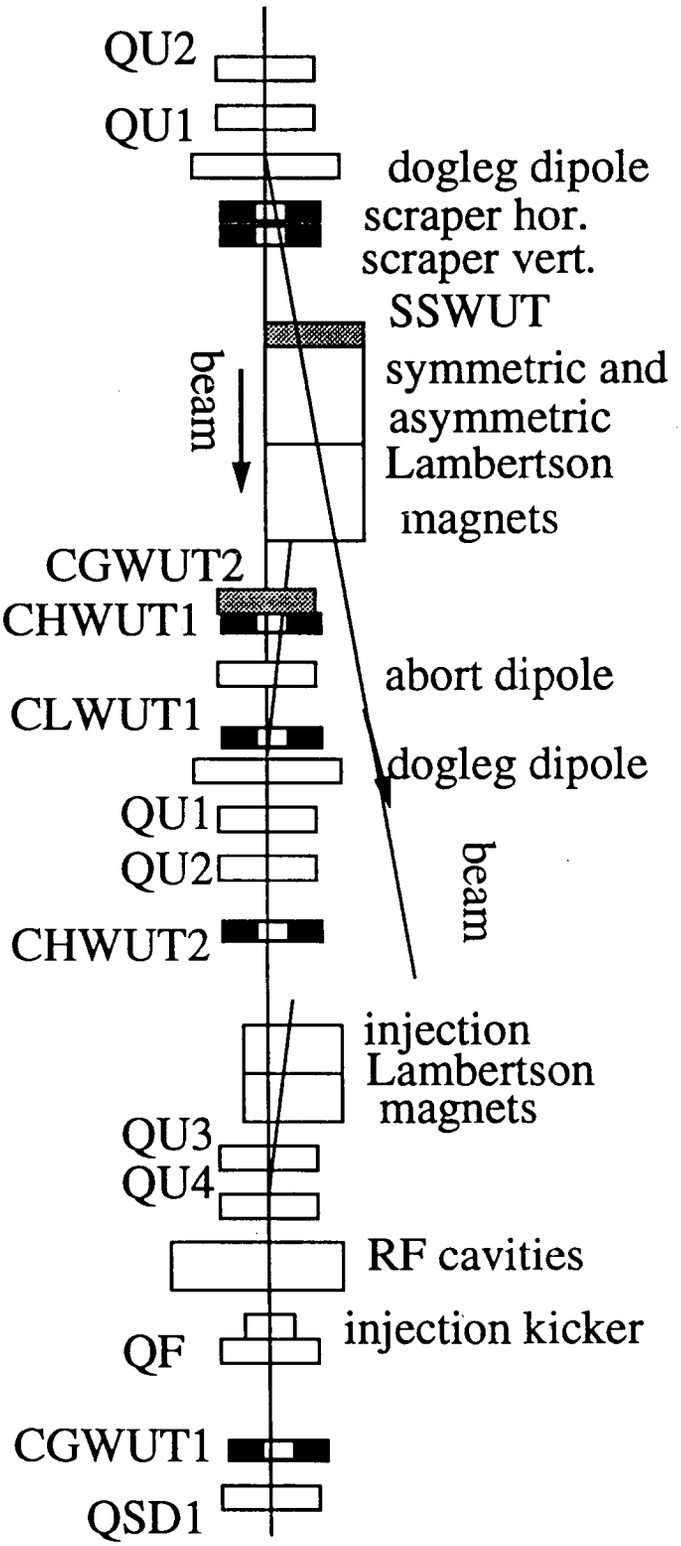

Fig. 1. Collimator locations in the Collider West Utility.

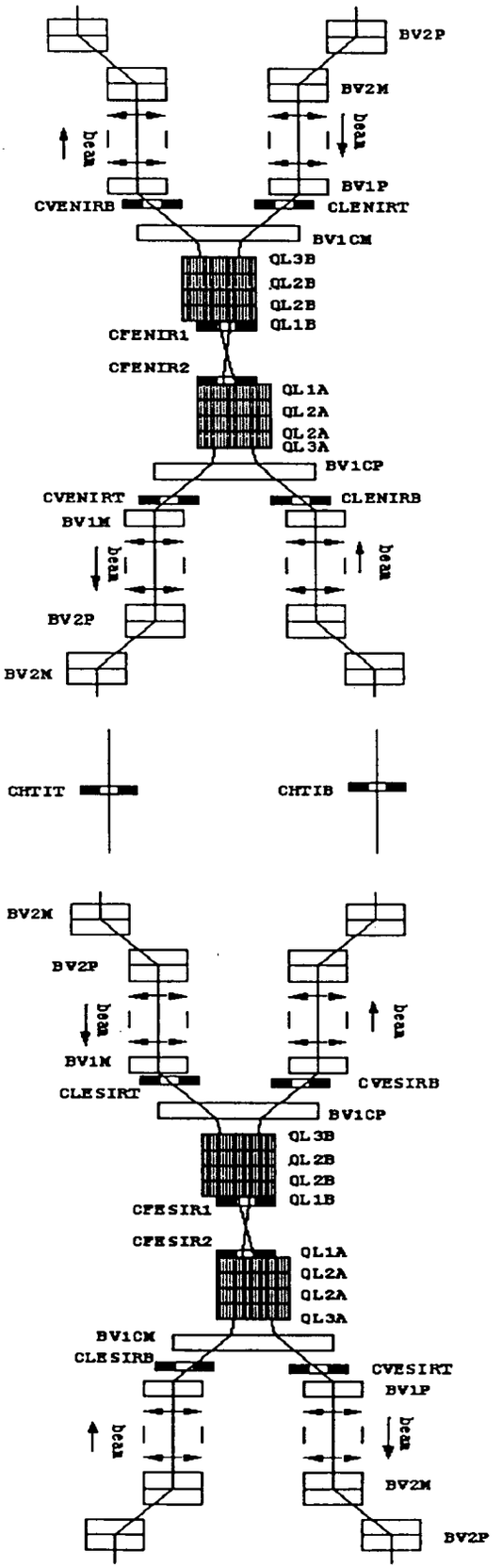

Fig. 2. Collimator locations in the Collider Interaction Regions.

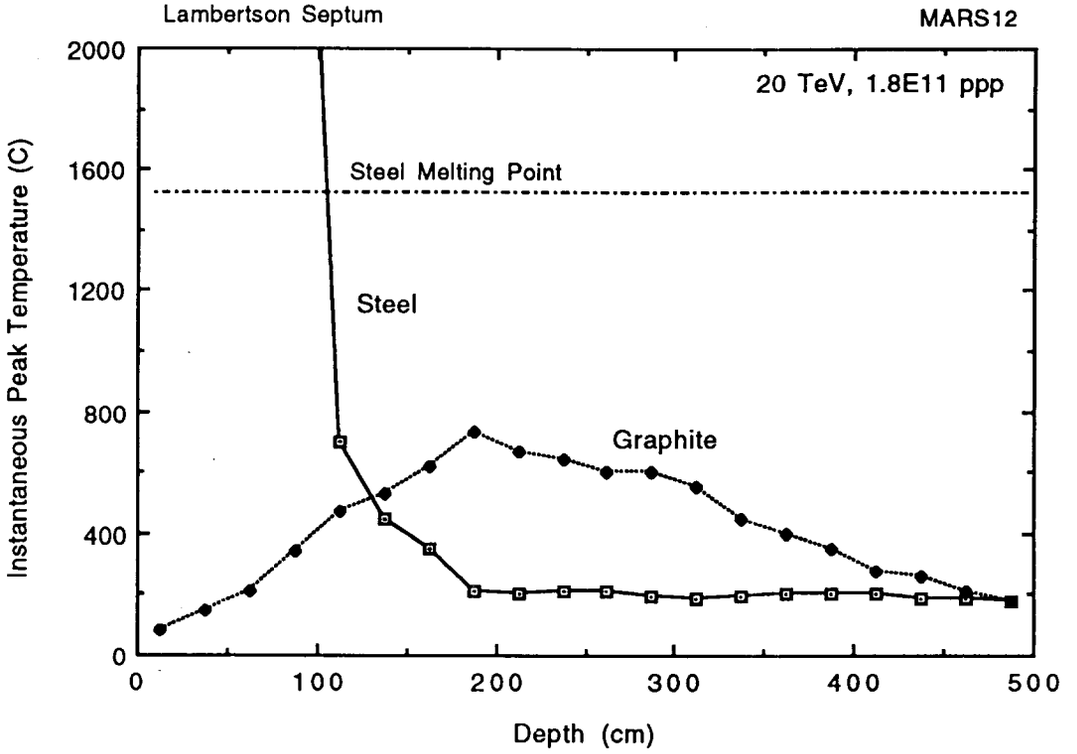

Fig. 3. Instantaneous maximum temperature in steel septum and graphite shadow vs depth at unsynchronized abort of 1.3×10^{14} protons with 20 TeV energy.

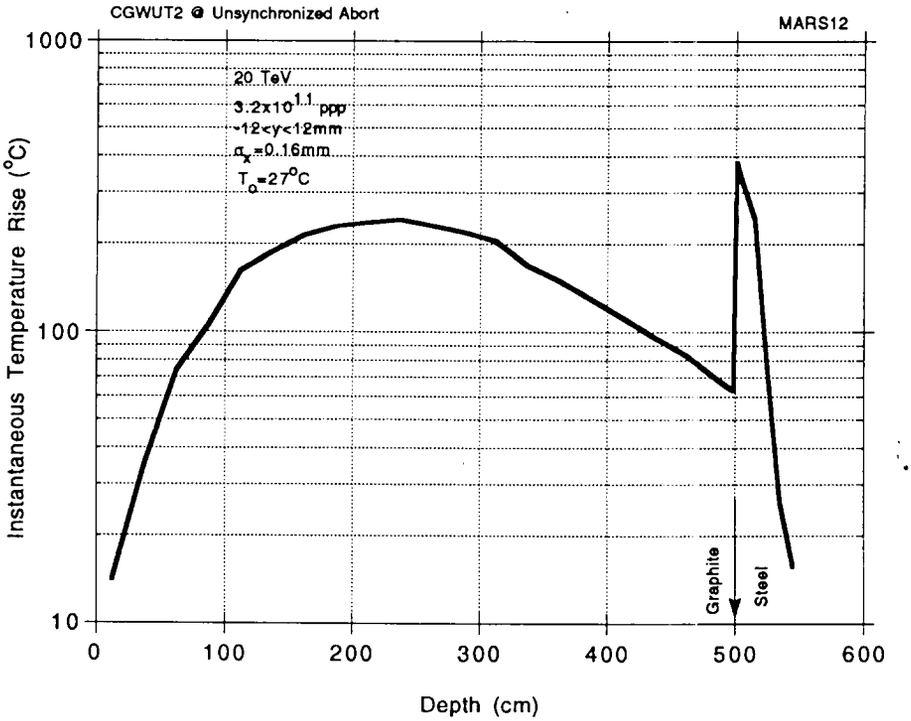

Fig. 4. Instantaneous maximum temperature in graphite shadow CGWUT2 followed by steel collimator at unsynchronized abort of 1.3×10^{14} protons with 20 TeV energy.

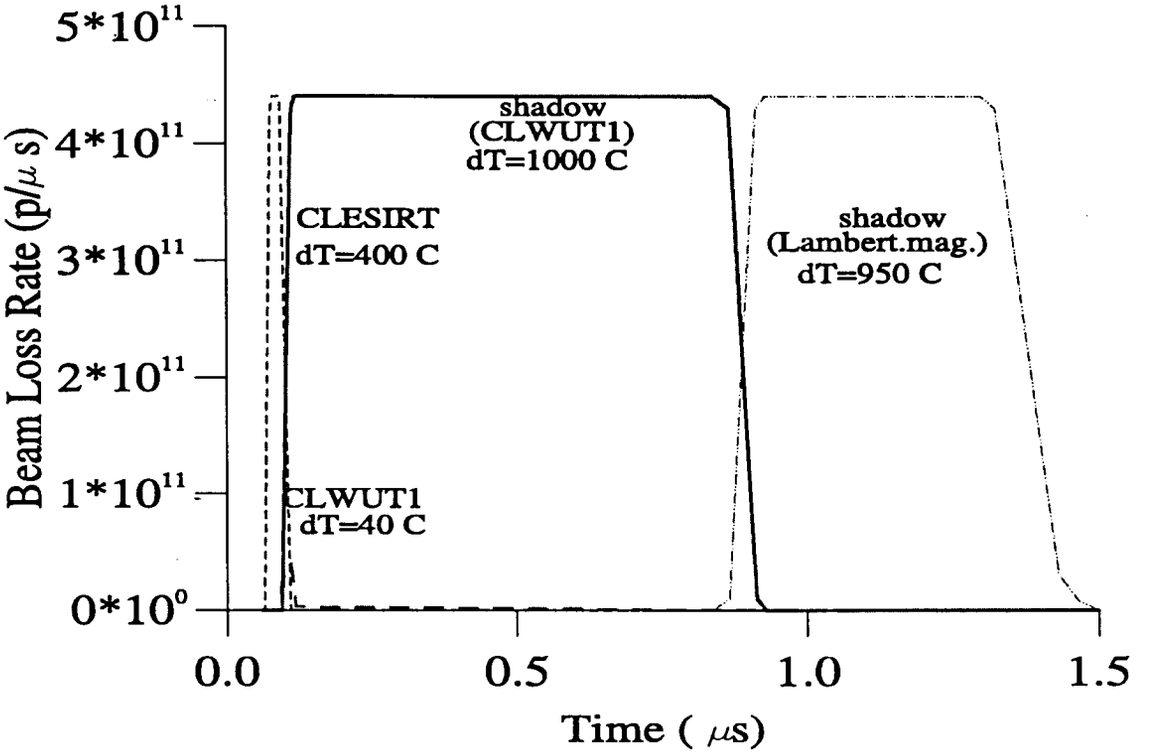

Fig. 5. Beam loss distribution during 3 μs collider kicker rise time at unsynchronized abort.

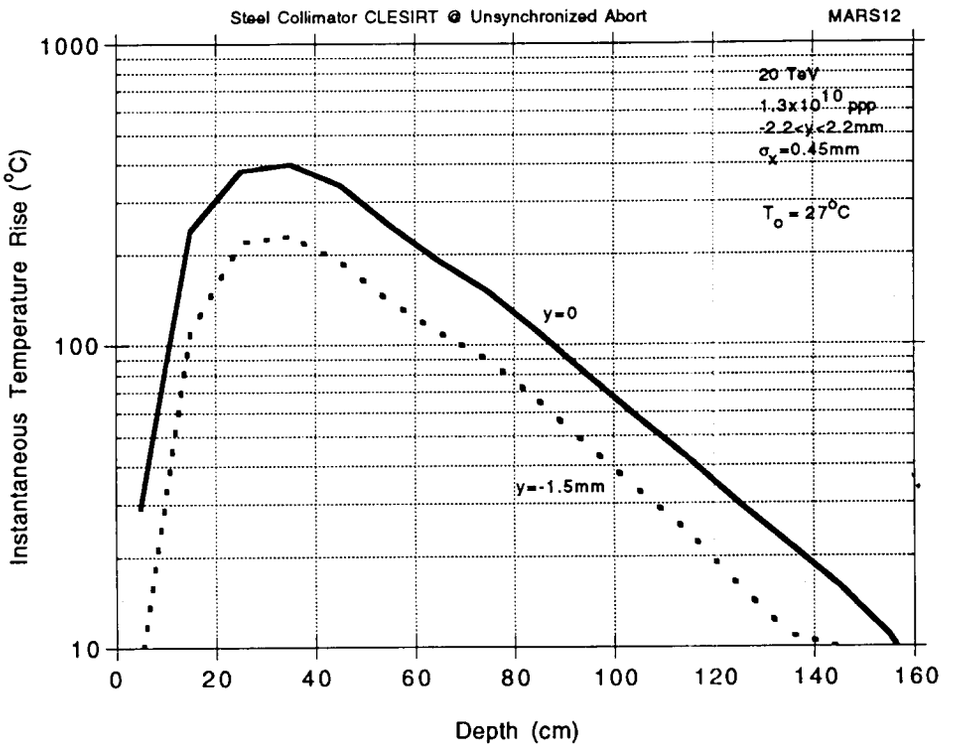

Fig. 6. Longitudinal temperature distribution in steel IR collimator CLESIRT at unsynchronized abort of 1.3×10^{14} protons with 20 TeV energy.

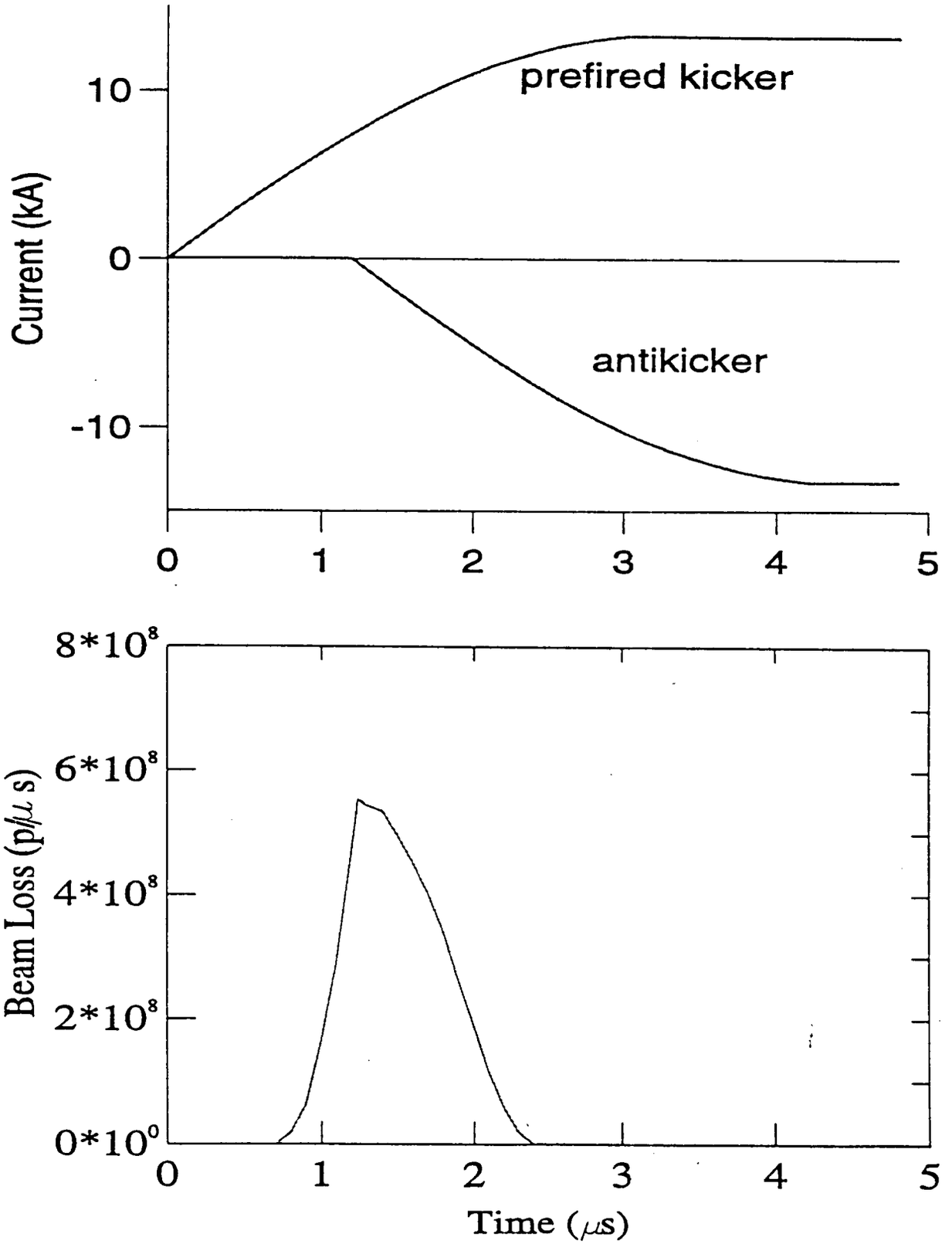

Fig. 7. Beam loss vs time for 1.2 μs antikicker delay.

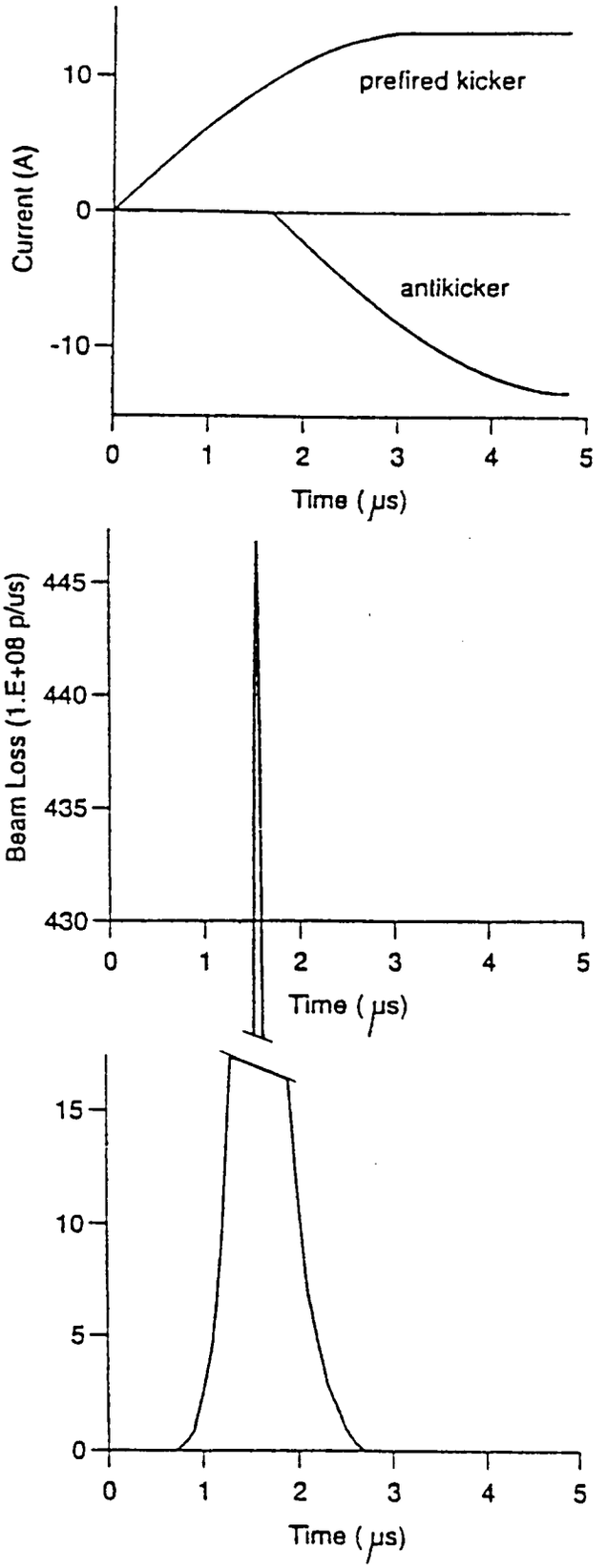

Fig. 8. Beam loss vs time for 1.65 μs antikicker delay.

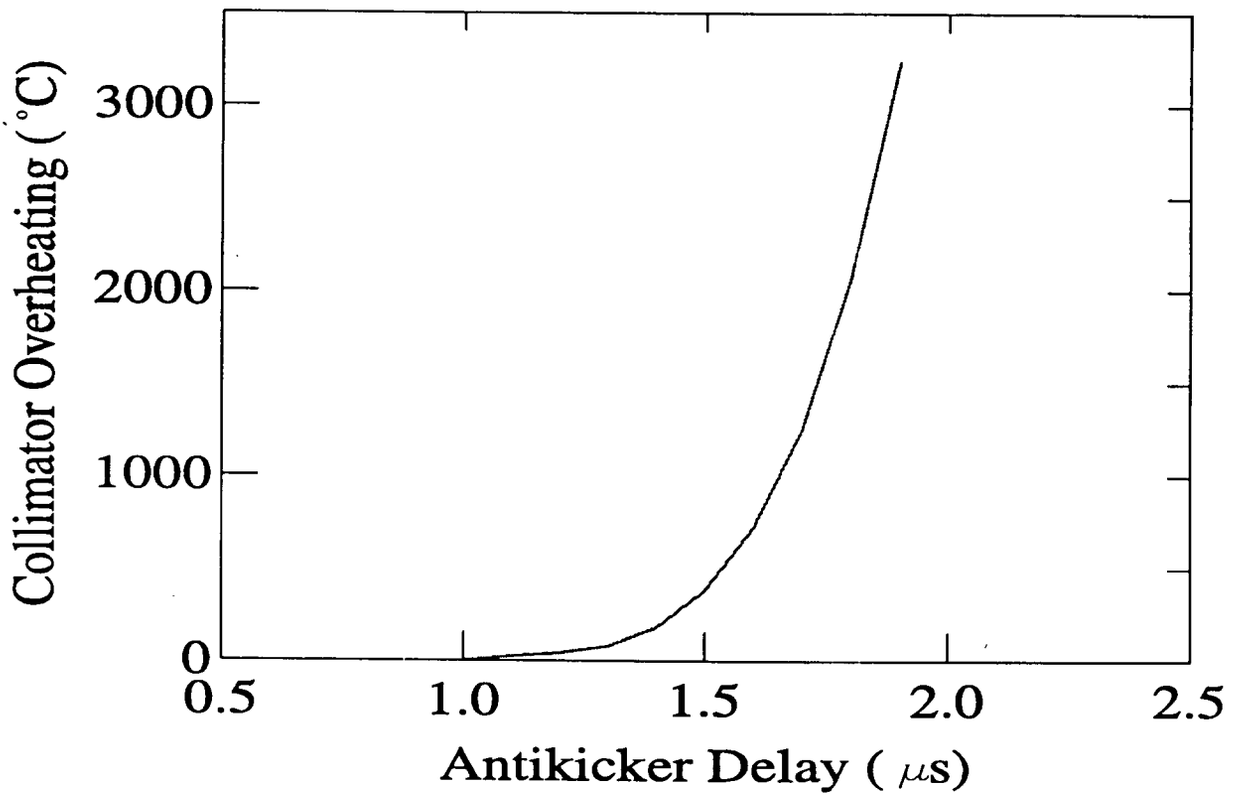

Fig. 9. Peak temperature rise in collimator jaws vs antikicker delay.

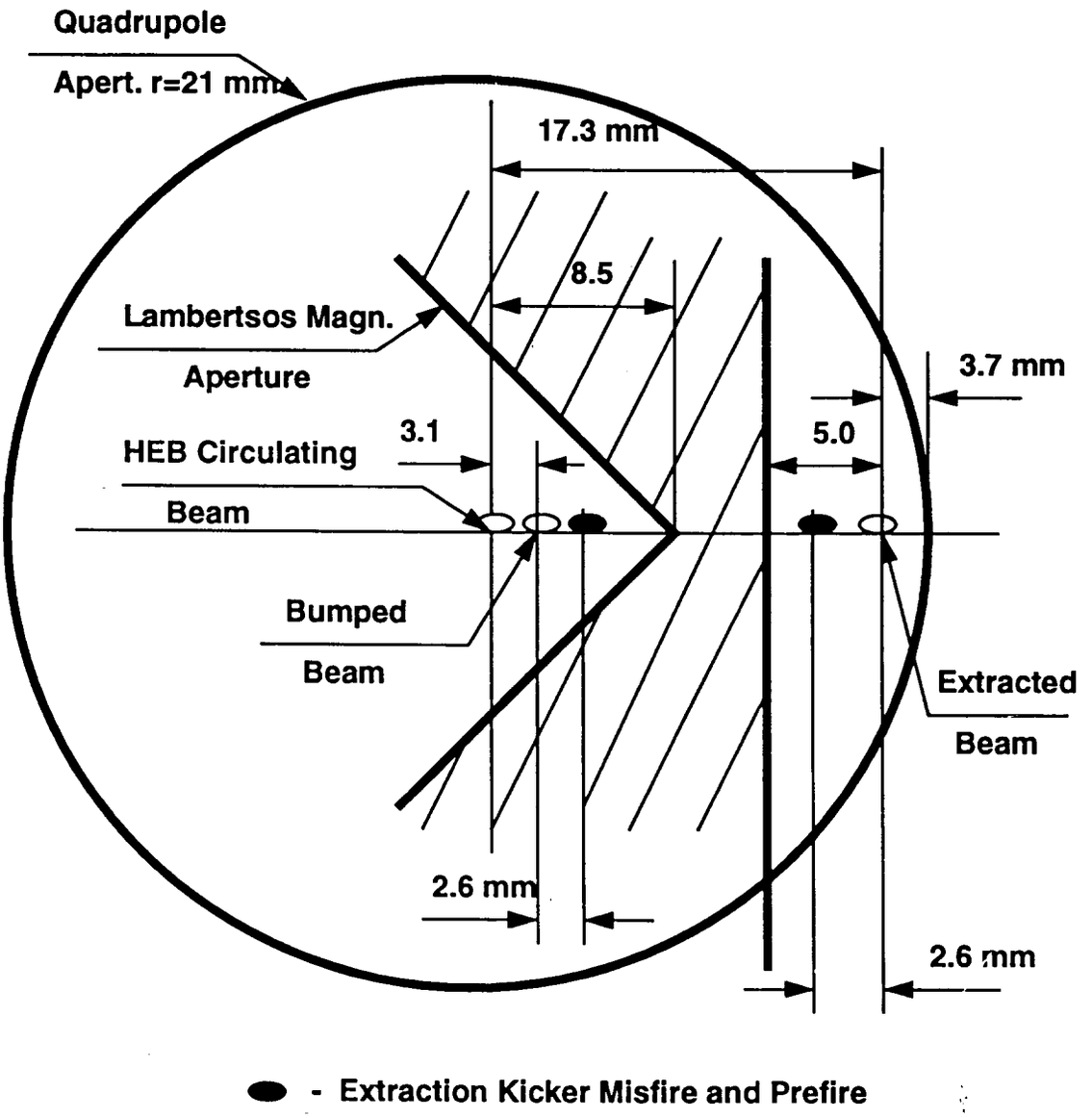

Fig.10. Beam positions at the upstream end of the HEB extraction Lambertson magnet.

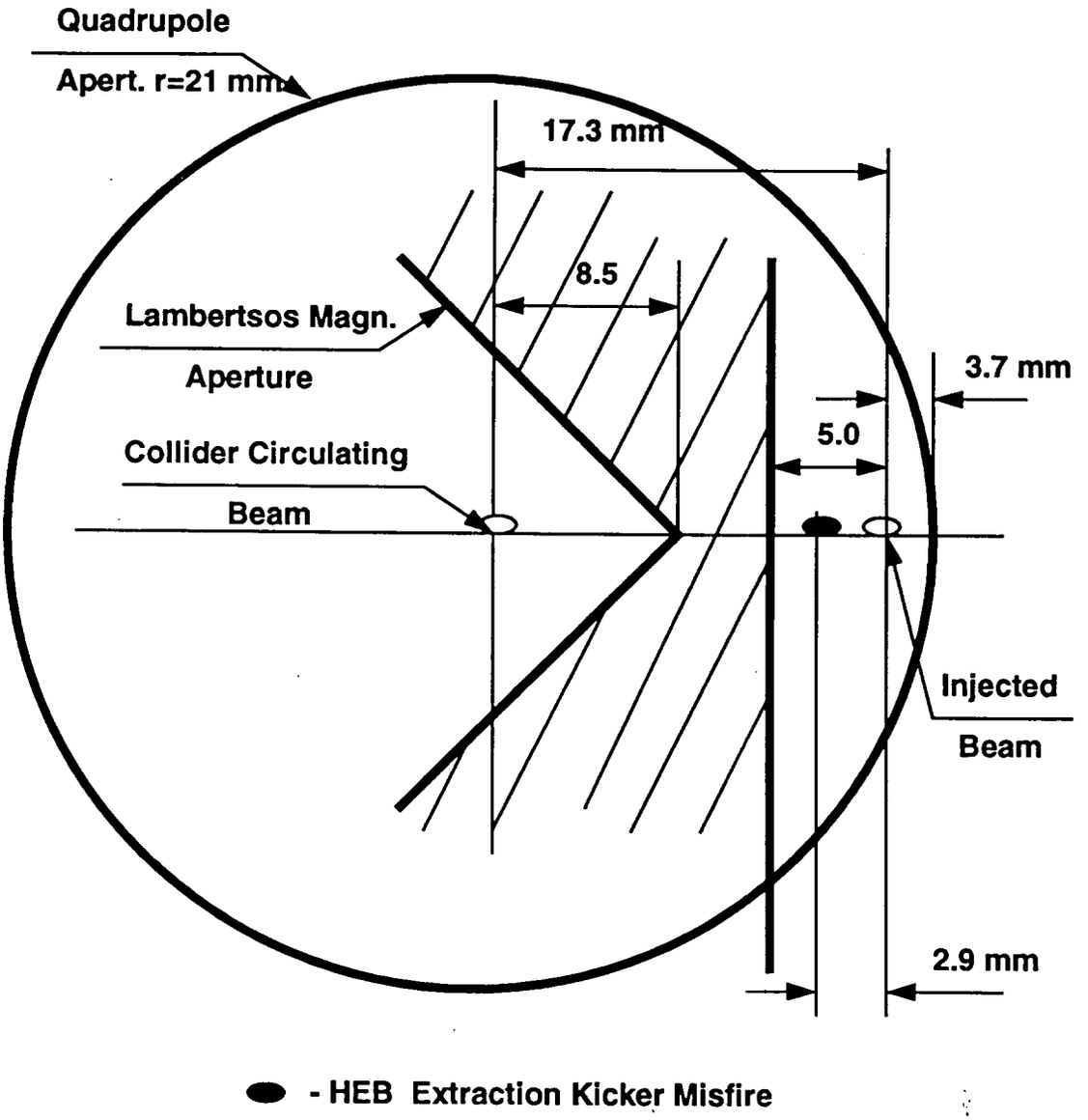

Fig.11.Beam positions at the downstream end of the collider injection Lambertson magnet.

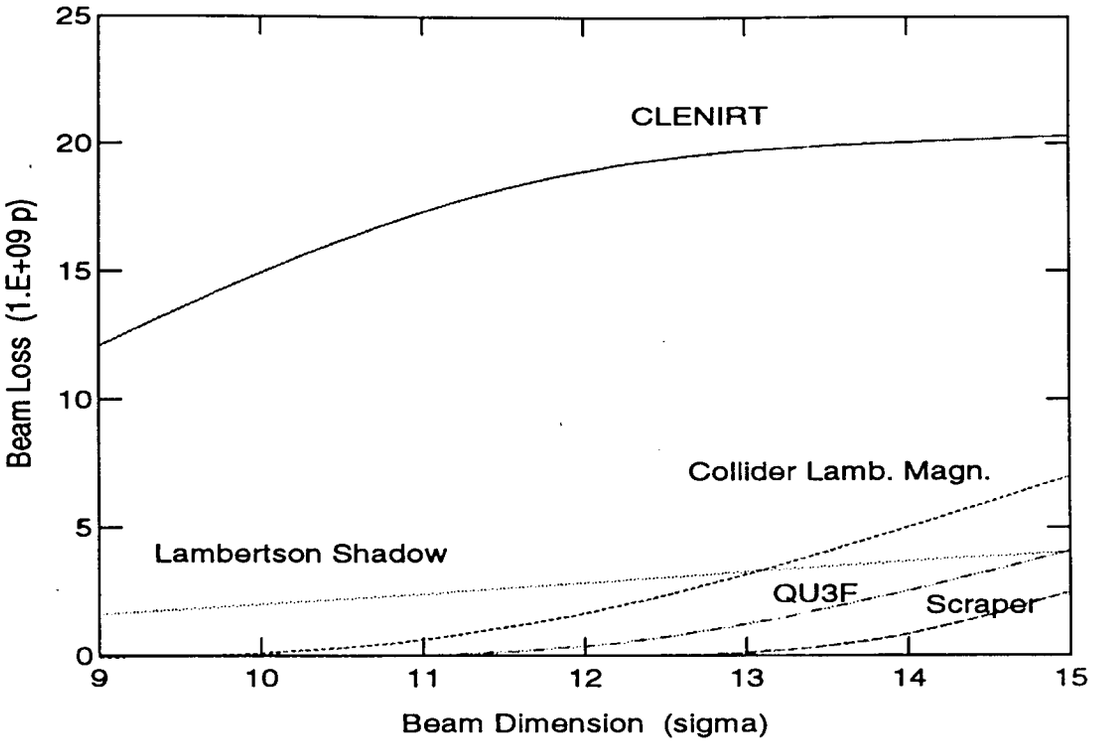

Fig.12. Beam loss at HEB extraction kicker misfire as a function of beam size. Injected beam is at 3 mm distance from Q1 and QU3B apertures.

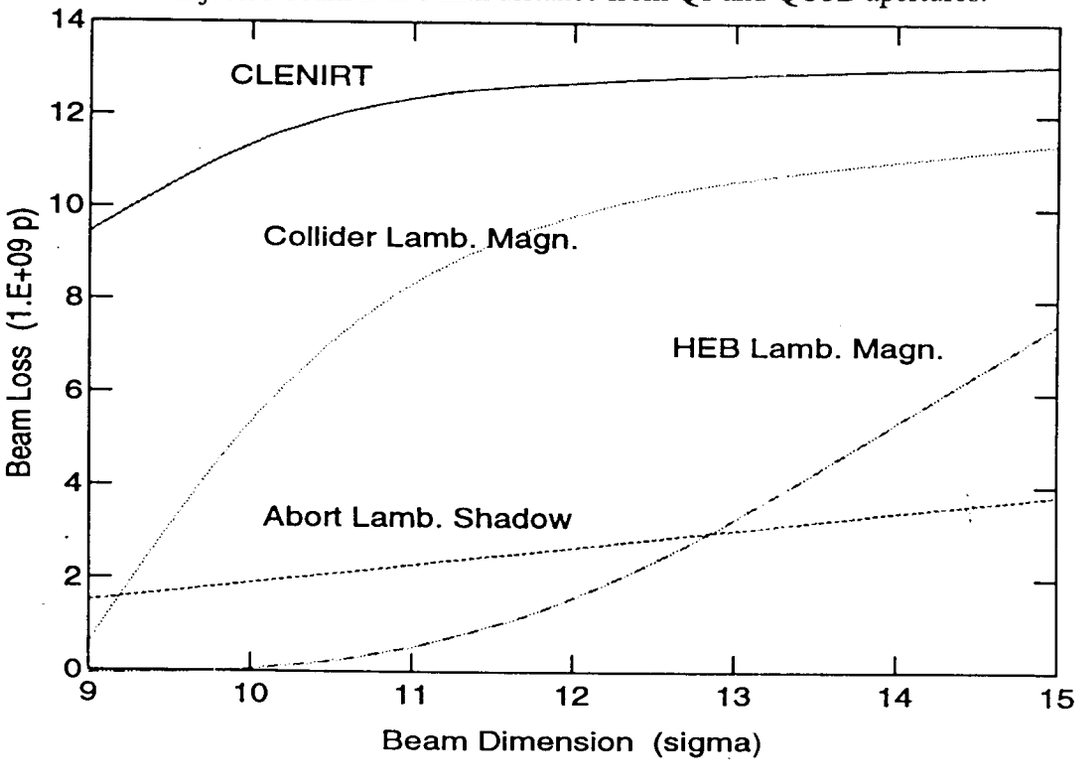

Fig.13. Beam loss at HEB extraction kicker misfire as a function of beam size. Injected beam is at 3.7 mm distance from Q1 and QU3B apertures.

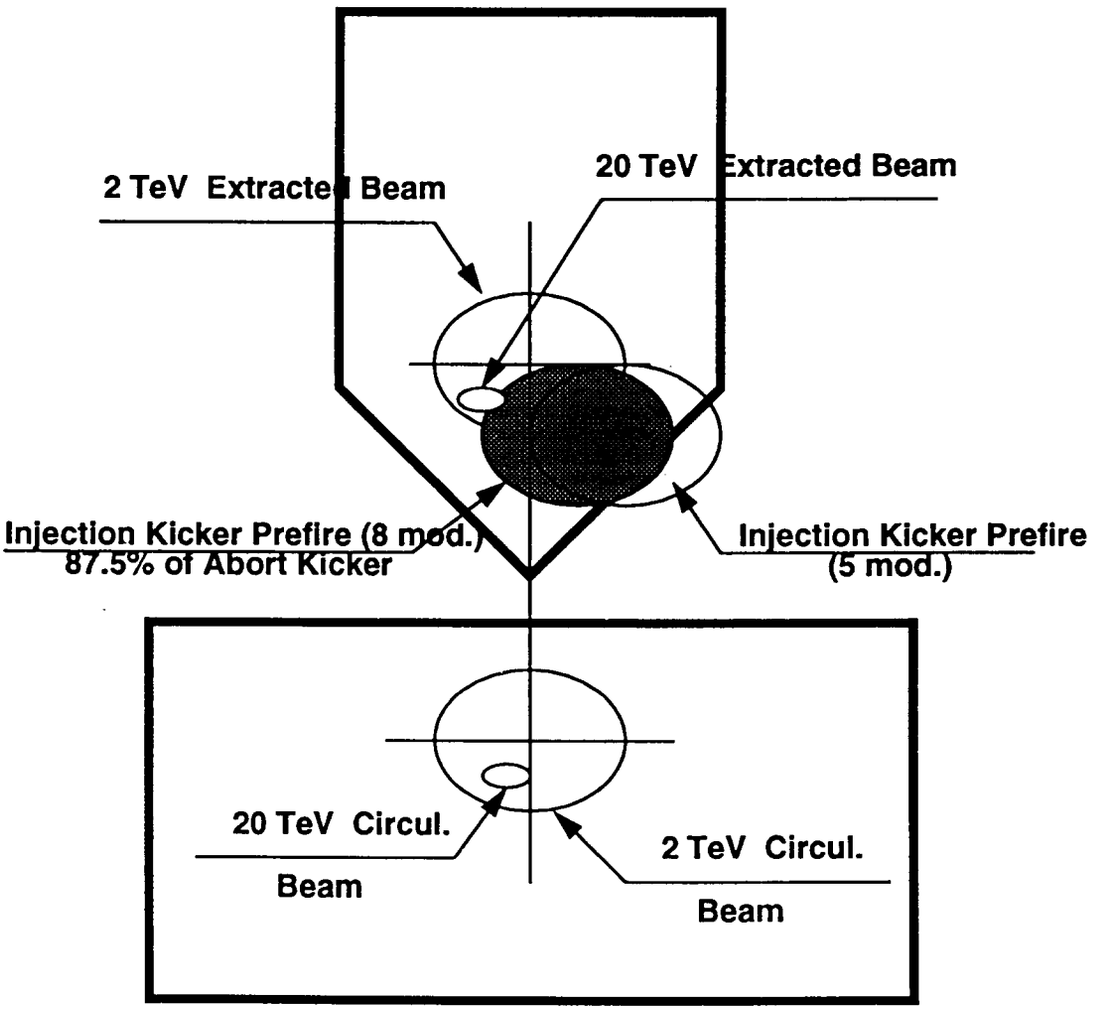

Fig.14. Circulating and aborted beam positions upstream the collider abort Lambertson shadow at injection kicker prefire.

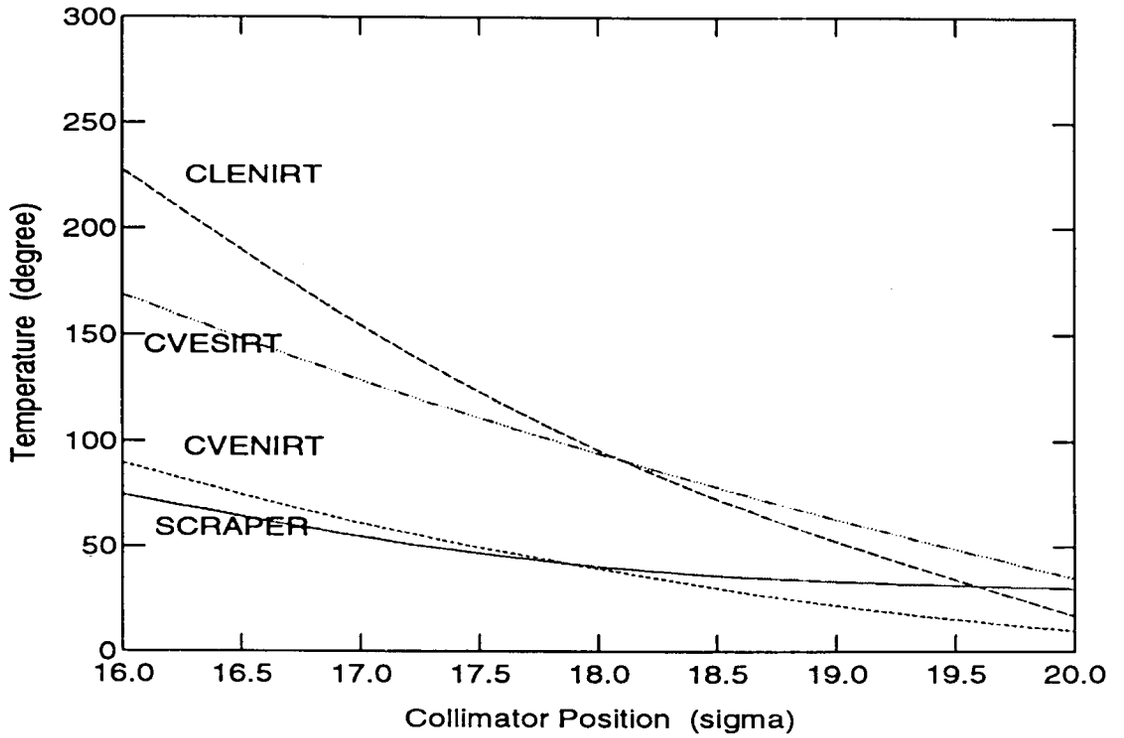

Fig.15. Peak instantaneous temperature rise in collimator at collider injectionkicker prefire and misfire vs jaw position. Kicker consists of 5 modules.

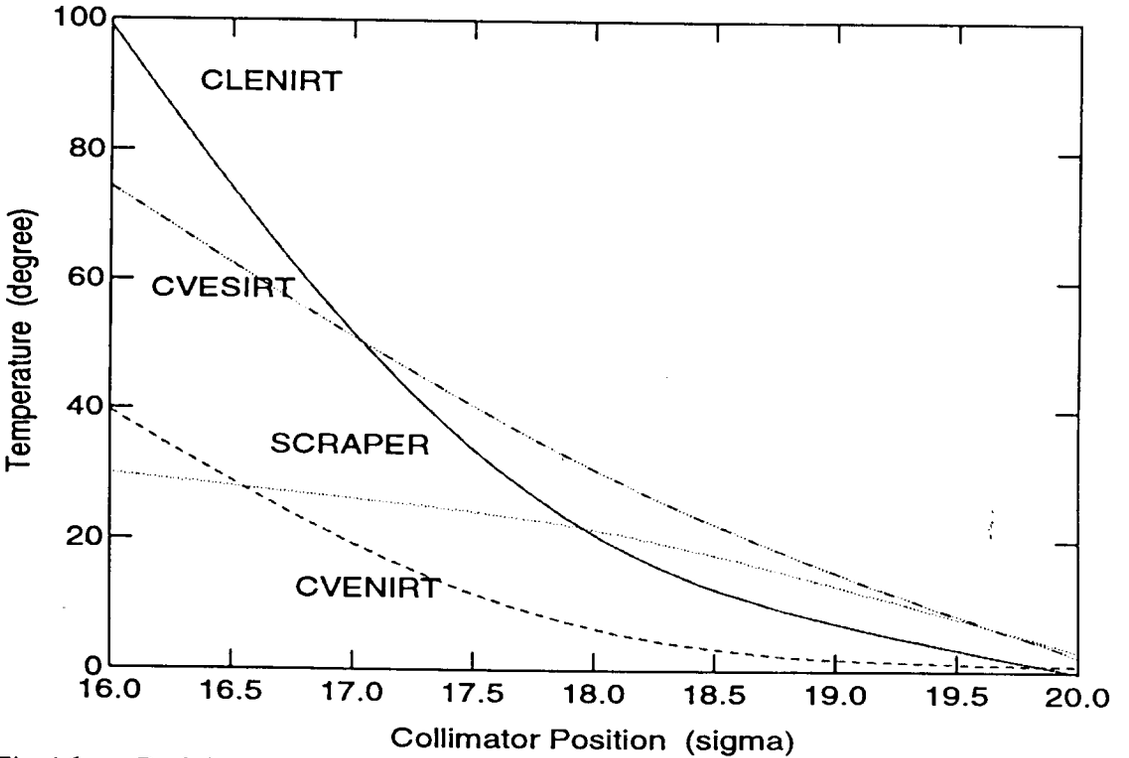

Fig.16. Peak instantaneous temperature rise in collimator at collider injection kicker prefire and misfire vs jaw position. Kicker consists of 6 modules.

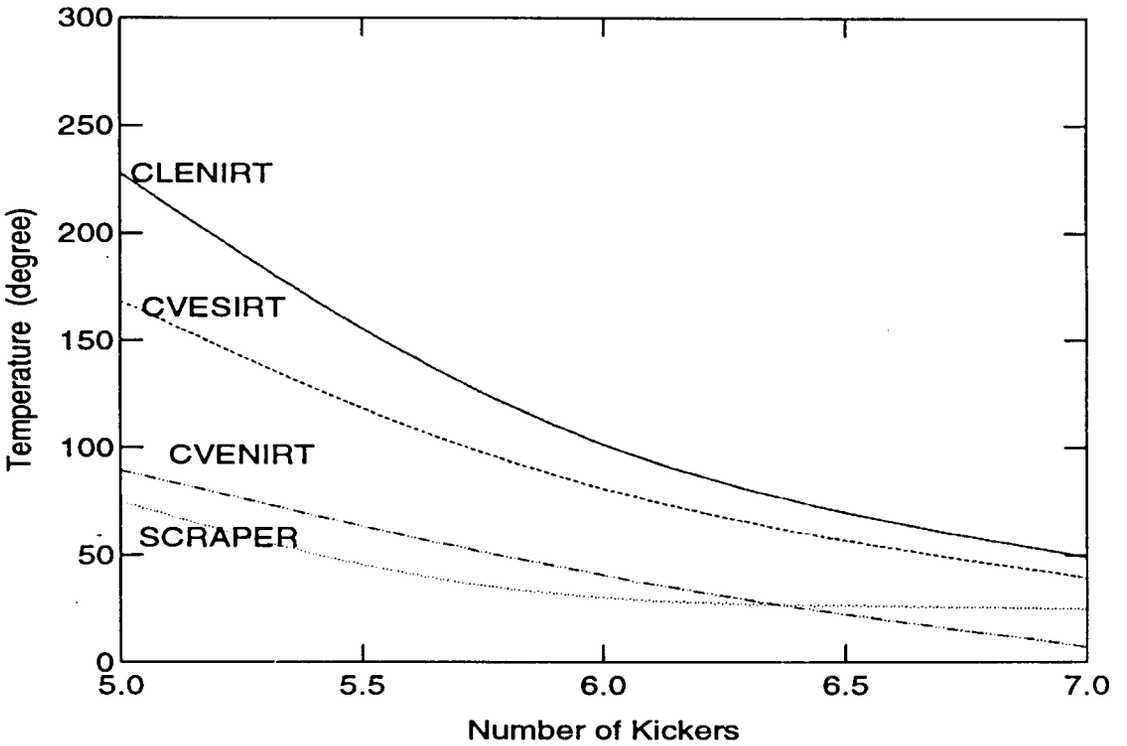

Fig.17. Peak instantaneous temperature rise in collimator at collider injection kicker prefire and misfire as a function of number of kicker modules.

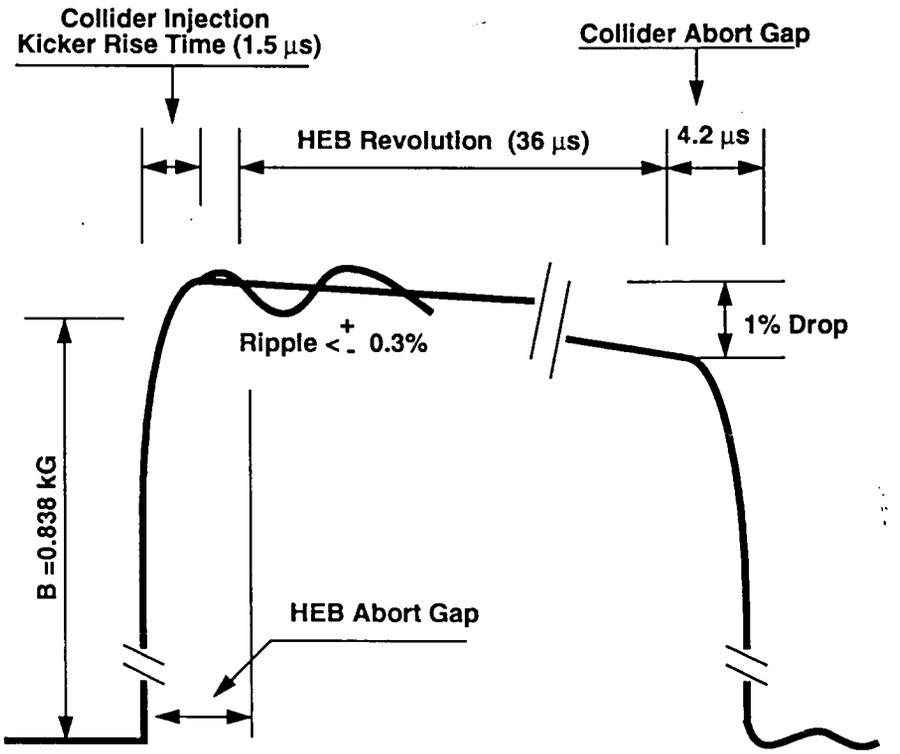

Fig.18. HEB extraction kicker pulse form.

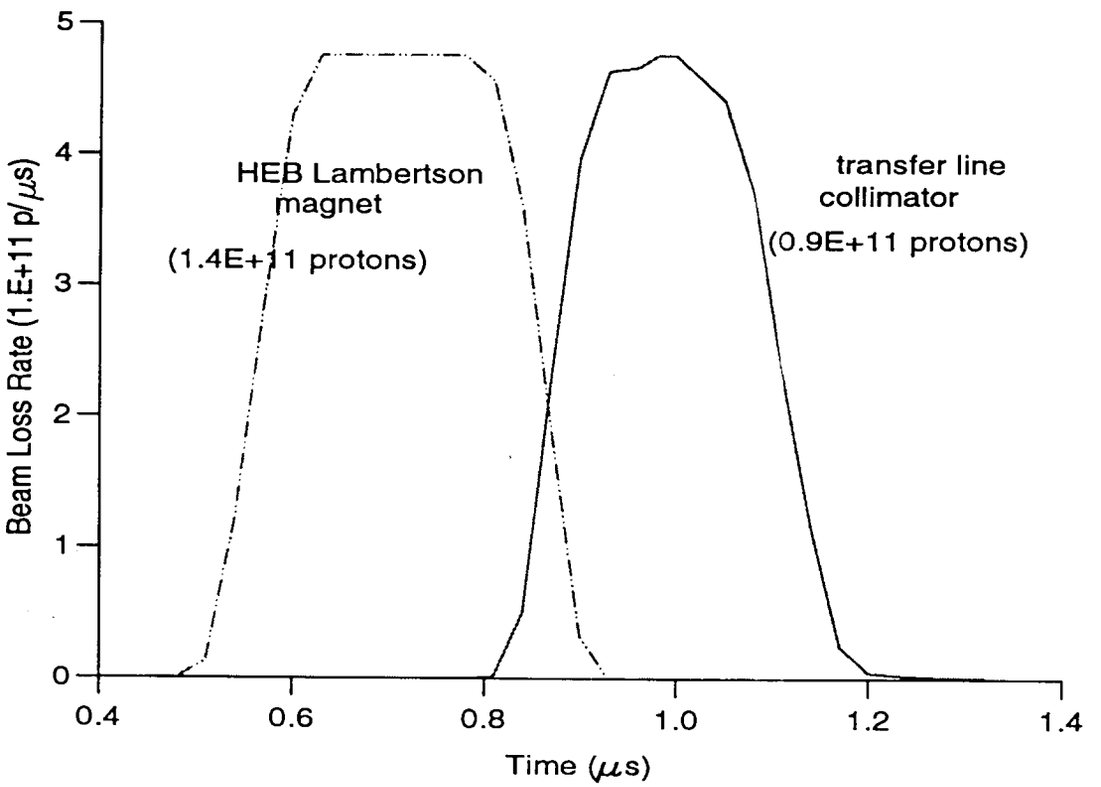

Fig.19. Beam loss at HEB extraction kicker timing errors.

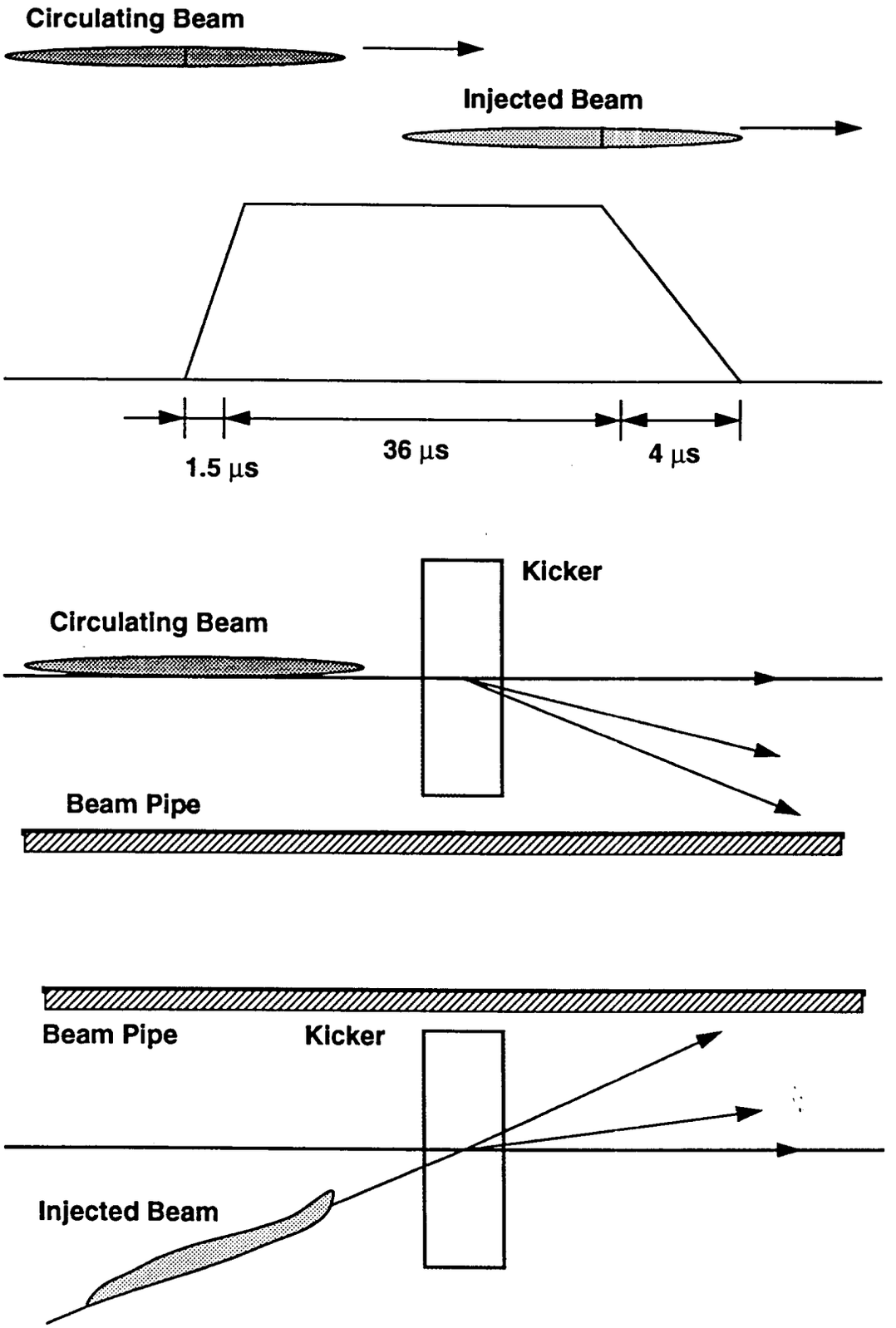

Fig.20. Scheme of beam loss at collider injection kicker timing error.

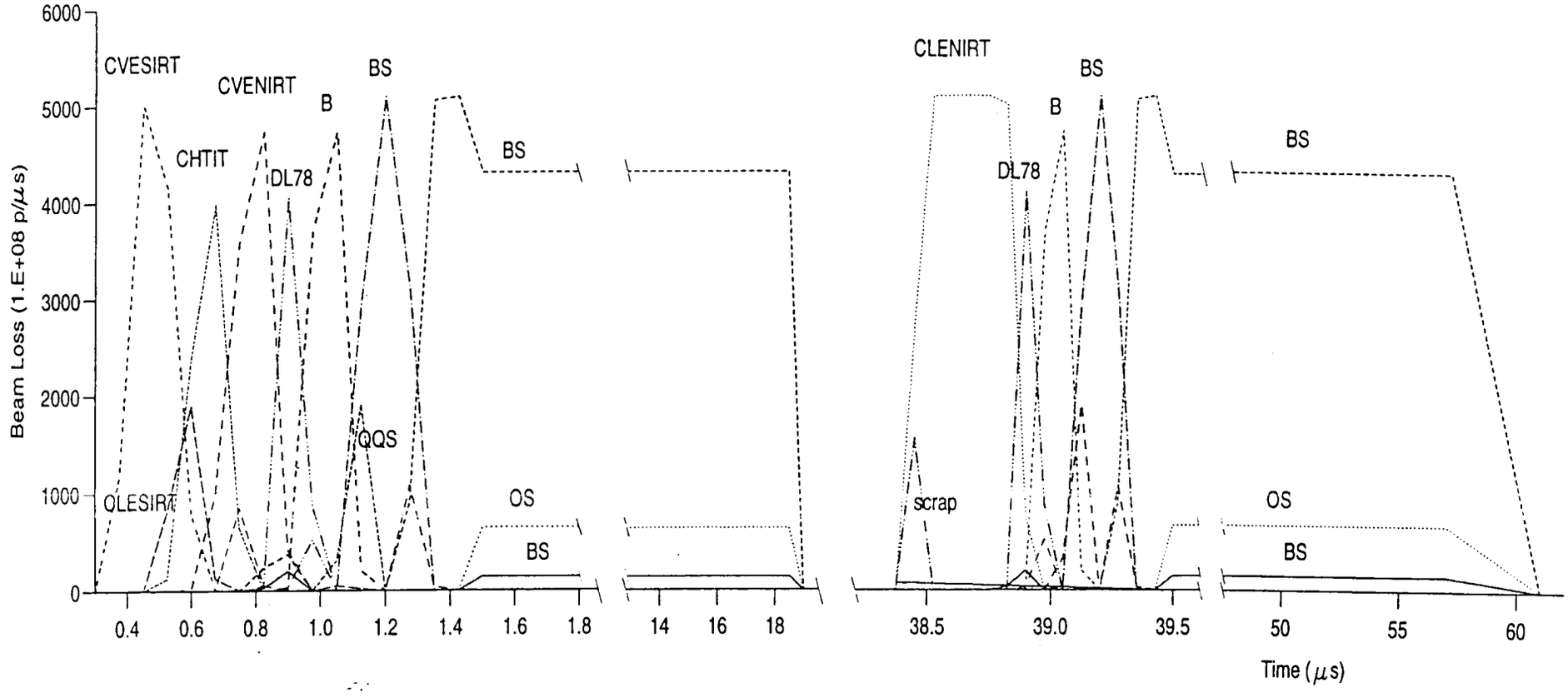

Fig.21. Beam loss at collider injection kicker timing error.

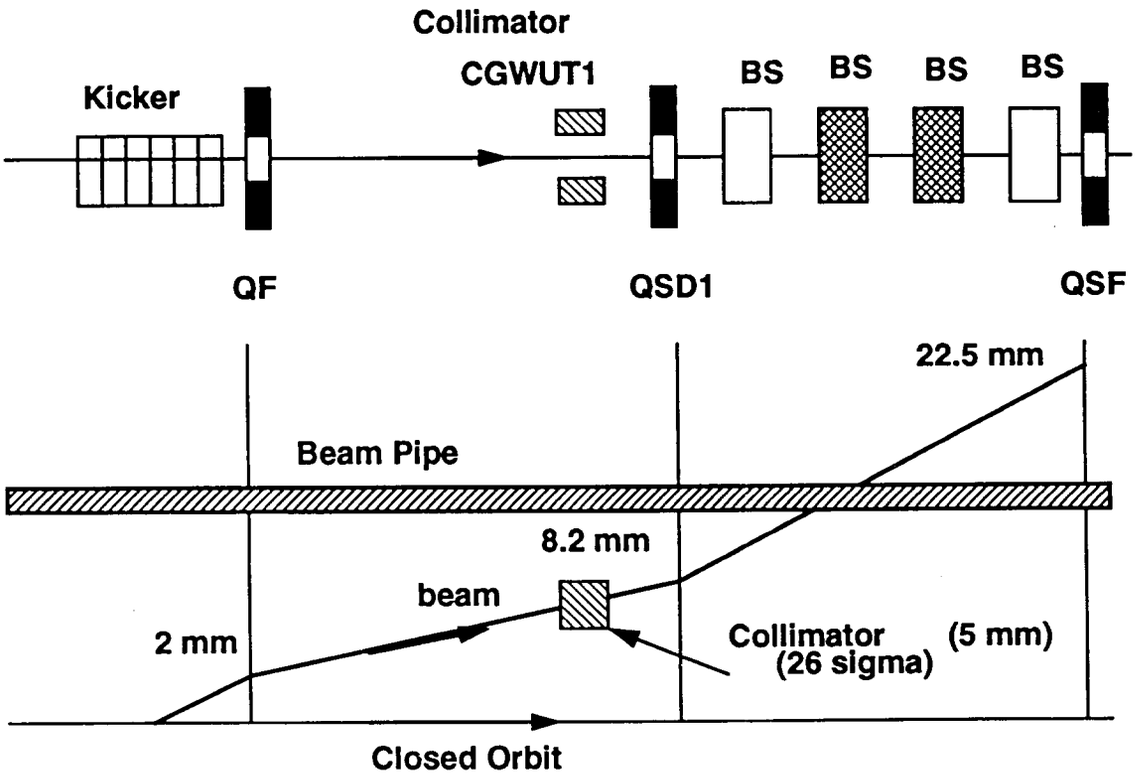

Fig.22. Fixed aperture collimator location downstream collider injection kicker.